Fracture Mechanics of Concrete Structures,
Proceedings FRAMCOS-2, edited by Folker H. Wittmann,
AEDIFICATIO Publishers, D-79104 Freiburg (1995)

WHAT IS INTERPRETED FROM FRACTURE SURFACES IN CONCRETE ?

H. Mihashi, N. Nomura and H. Nakamura
Department of Architecture, Tohoku University, Sendai, Japan
T. Umeoka
Nagoya Branch of Shimizu Co., Nagoya, Japan

Abstract
Based on a three-dimensional spatial measurement, several parameters to analyze quantitatively features of fracture surfaces in different types of cementitious composite materials are presented. The parameters are ratio of real surface area to the projected area, interface area, orientation of facets in the fracture surface, surface fractal dimension, and line fractal dimension. Then the fracture properties and resisting mechanisms are discussed with relation to these parameters.

1 Introduction

It has been generally accepted that crack growth in concrete is associated with a nonlinear region in front of the crack tip, called fracture process zone (FPZ), but its detailed mechanisms are still ambiguous. While fracture energy G_F has been found to be a nonlinear fracture mechanics parameter to represent the crack resisting properties of concrete, G_F is defined as the energy absorbed to create a unite area of projected fracture surface (RILEM, 1985). Studies on FPZ such as the crack face bridging in concrete by Van Mier (1991), microcracks in terms of three-dimensional acoustic emission by Mihashi and Nomura (1992a), and visualization by means of X-ray technique by Otsuka (1994) suggested that there are many cracks occurred inside from the final fracture surfaces on fully separated specimens and that topological measurements of the surface are not sufficient to characterize the whole fracture mechanisms. However, many researchers often experience that large amount of G_F is usually gained in concrete whose fracture surfaces are very rough. Sometimes the cause of large fracture energy is explained by the increasing real fracture surface, though any qualitative studies have not proved it yet. It may mean that a certain information about the fracture properties is still hidden in the features of fracture surfaces. For example, Mecholsky et al. (1989) showed that the fractal dimension is related to the toughness of aluminum and glass-ceramics.

The objective of this paper is to study parameters which can quantify the characteristics of features in the fracture surface such as ratio of real surface area to the projected area, interface area, orientation of facets in the fracture surface, surface fractal dimension, and line fractal dimension as well as distributions of these parameters.

2 Analytical procedures of fracture surfaces

2.1 Measurement of fracture surface

Elevation of fracture surfaces is measured by means of a laser displacement censor (Fig. 1) at intervals of 0.2 or 0.4 mm which constructs a fracture surface map as triangular network of 251x251 mesh data (Fig. 2) to digitize the realistic fracture surface.

Since it is hardly possible to characterize features of fracture surfaces in concrete excluding the influence of aggregates in order to study the fracture mechanism, image information of aggregates is essential to be combined.

By means of a video camera, the photographs are input into the image processing apparatus in which the analogue information of 100x100 mm^2 is transformed into 800x800 picture elements to get a binary digital image information. Then on the basis of linear transformation, these digital images are correlated to the mesh data. These treatments relate the location, shape and size of mortar-aggregate interfaces and/or broken aggregates to the fracture surface map.

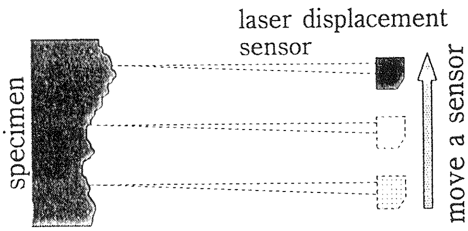

Fig.1 Measurement of surface

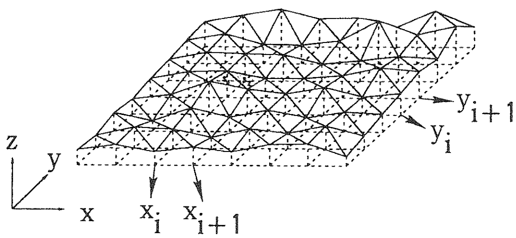

Fig.2 Fracture surface map

2.2 Fracture surface area

The basic problem in quantifying the true magnitudes of features in the nonplanar fracture surface is that the elevation information and the area of a fracture surface must be known. In case of cementitious composite materials, the summation of areas of triangular elements could be the estimation of fracture surface area. Although this procedure allows the fracture surface area to be estimated, it is essentially no more than an approximation of the complex and irregular fracture surfaces. The apparent measured area of the same fracture surface obviously increases as the interval size decreases.

2.3 Fractal dimension

It is well-known that ordinary measurements become meaningless to measure complex curves and surfaces. There is a way, however, to measure the degree of the complexity by evaluating how fast the length, or the surface area increases with the measurement of smaller and smaller scales. The fundamental idea is to assume that the two quantities, - i.e. length or surface, and scale - don't vary arbitrarily but rather are related by a law. The kind of law which seems to be relevant is a power law of the form $y \propto X^D$ and the exponent D is called fractal dimension.

Surface fractal dimension D_S is determined by eq.(1) (Fig. 3) and line fractal dimension D_L is determined by eq.(2).

$$S(\eta^2) = S_0 \cdot (\eta^2)^{-\frac{D_S - 2}{2}} \tag{1}$$

$$L(\eta) = L_0 \cdot \eta^{-(D_L - 1)} \tag{2}$$

where η is the mesh size to measure, $S(\eta^2)$ is the area and $L(\eta)$ is the length measured with the mesh size η , S_0 and L_0 are constants. D_L represents the roughness properties of a profile, while Ds describes the properties of the whole surface. In this study, variation of D_L was measured for scanning lines in two directions on the fracture surface

(Fig. 4) besides Ds. Although the most popular block counting method was also applied to analyze the surface fractal dimension, the accuracy was much lower than that of the present method.

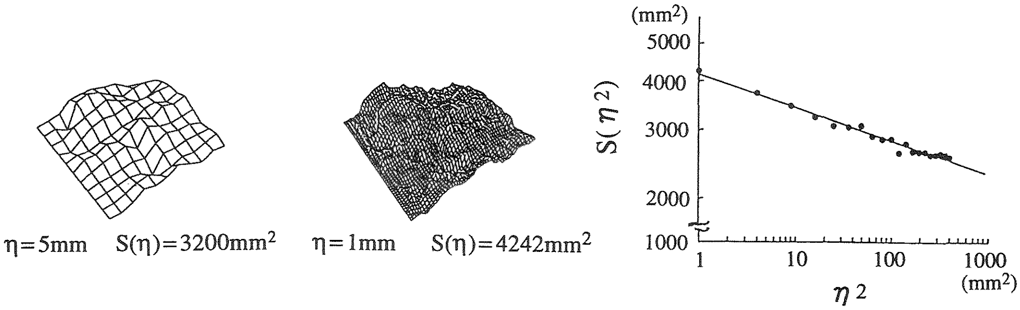

Fig.3 Suraface fractal dimension

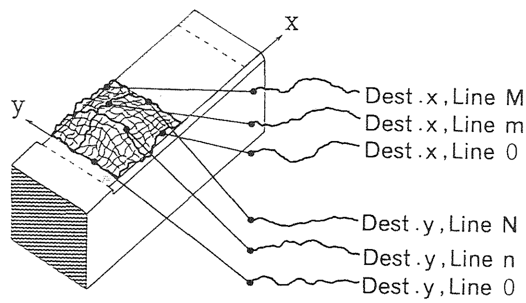

Fig.4 Scanning lines for fractal dimension

2.4 Roughness parameter

If the roughness parameter is known, it may enable simple relationships to be set up for features in the fracture surface. The surface roughness parameter (Rs) is defined by eq.(3).

$$Rs = S_f/A' \tag{3}$$

where S_f is the surface area measured with the finest mesh size and A' is projected area of the fracture surface.

2.5 Distribution of facet orientation

Once the fracture surface map is obtained, orientation of a facet which is a triangular small surface in the map can be analyzed with angles θ and ϕ defined in Fig. 5. These angles were evaluated as the mean values of every 5 meshes in this study.

When the fracture surface is very rough, the angle θ distributes very closely to 90°. On the other hand, θ is almost 0° when the fracture behavior is brittle and the surface is very flat. If θ of all facets are $0°$, the whole fracture mode is purely Mode I. If not, mixed mode fracture locally occurred in the fracture process.

Angle ϕ shows the orientation of cracking. For example, $\phi=0°$ or $180°$ is observed when the crack deflects around an inclusion (Fig. 6). From the probability density function (PDF) of ϕ, the fracture mode may be subdivided into three patterns as shown in Fig. 7. Pattern I is related to a brittle fracture, pattern II is caused by local deflection due to uniformly distributed inclusions, and pattern III has relevance to random deflection caused by quite heterogeneous structures.

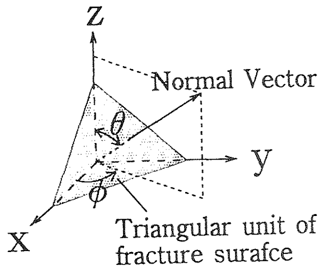

Fig.5 Definition of angle

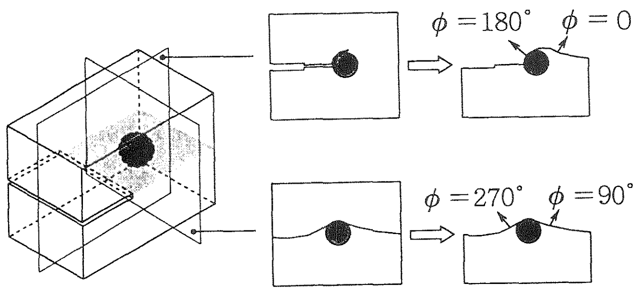

Fig.6 Angle ϕ and crack deflection

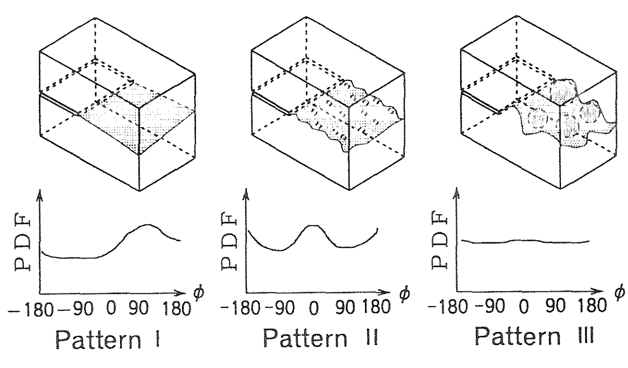

Fig.7 Fracture patterns defined with angle ϕ

3 Outline of test series

In this study, there are three test series experimented to analyze features of the fracture surface as follows:

Series I: Wedge splitting tests of mortar reinforced with short fibers,

Series II: Double cantilever beam tests of concrete with different aggregate size,

Series III: Three-point-bend tests of notched beams of concrete of three different strength levels.

In Series I, three types of chopped fiber were contained in fiber reinforced mortar, which were high modulus PVA (vinylon) in specimen VINYL, pitch type carbon fiber in specimen PITCH, and PAN type carbon fiber in specimens PAN and PANSI(with silicafume by the weight of 30%). The volume content of all these fibers were 3%. Properties of these fibers are given in Table 1. Water-cement ratio was 0.40 and sand-cement ratio was 1.5. Geometry and dimension of the fracture surface is shown in Fig. 8. The elevation of the fracture surface was measured at intervals of 0.2mm. More details of the testing conditions are shown in Mihashi et al. (1992b).

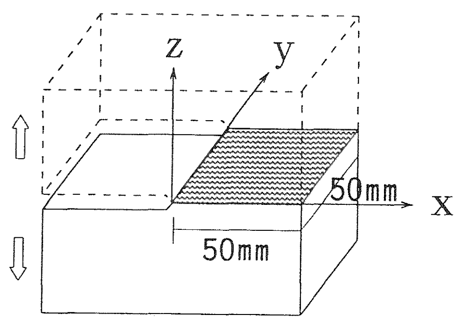

Fig.8 Dimension of fracture surface in Series I

Table 1. Properties of fiber

Fiber/Type	Length(mm)	E(MPa)	ft(MPa)	Elongation(%)
Carbon/PAN	6	235000	4217	1.8
Carbon/pitch	6	33000	790	2.4
PVA/Vinylon-AA	6	39500	1834	6.7

In Series II, mortar and plain concrete containing only a certain range of gravel grain size were tested (Table 2). Geometry of the specimen is shown in Fig. 9. While the size of fracture surface 250x100 mm^2 was too wide to measure, following the crack propagation process, the first 100x100 mm^2 part (Par I) close to the notch tip and the second

100x100 mm2 part (Part P) close to the edge were planned to measure at intervals of 0.4mm. According to results of AE monitoring (Mihashi et al. 1992a), the head of the FPZ is located at about 90 mm distanced from the notch tip independently of the aggregate size when the maximum load was recorded. Therefore the Part I may contain some informations of whole fracture process, and the Part P may relate only to the fracture process of descending part in the load-deflection curve.

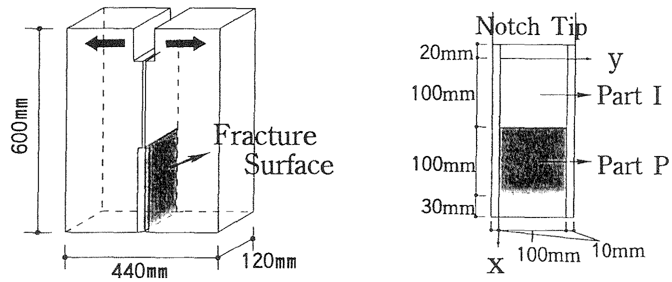

Fig.9 Geometry of specimen in Series II

Table 2. Mix proportion and compressive strength in Series II

Group	Size(mm)	G(kg/m³)	S(kg/m³)	C(kg/m³)	fc(MPa)
AEM2	-5	-	1146	740	40.4
AEC101	5-10	925	722	460	34.8
AEC151	10-15	936	722	460	33.3
AEC201	15-20	939	722	460	30.5
AEC301	20-30	939	722	460	24.9
AEC302	20-30	939	722	460	24.9

In Series III, size and volume of coarse aggregates were kept constant but strength of mortar was changed. Mix proportion and strength of concrete are shown in Table 3. Superplasticizer was used in high and medium strength concrete. The geometry of the specimen is shown in Fig. 10. Fracture surface was treated as two parts whose size was 50x50mm2. Each part were measured at intervals of 0.2mm.

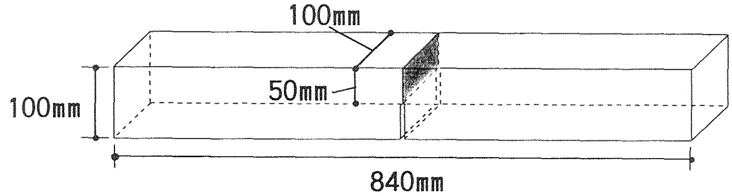

Fig.10 Geometry of specimen in Series III

Table 3 Mix proportion of concrete in Series III

Group	dmax(mm)	W/(C+Si)	W(kg/m^3)	C(kg/m^3)	S(kg/m^3)	G (kg/m^3)	Si(kg/m^3)	fc (MPa)
A2	25	0.65	227	349	721	1006	0	21.4
A5	25	0.4	160	340	721	1006	60	64.5
A10	25	0.2	111	444	721	1006	111	96.4
B2	5	0.65	227	349	721	1006	0	20.9
B5	5	0.4	160	340	721	1006	60	58.8
B1	5	0.2	111	444	721	1006	111	105.9
C2	-	0.65	227	349	721	0	0	33.8
C5	-	0.4	160	340	721	0	60	46.3
C1	-	0.2	111	444	721	0	111	110.7

4 Results and discussion

4.1 Fractal dimension and roughness parameter

Surface fractal dimension Ds, line fractal dimension in two directions (D_{Lx}, D_{Ly}) and roughness parameter Rs of each fracture surface were analyzed as shown in Appendix (Table A-1). Generally speaking Ds is

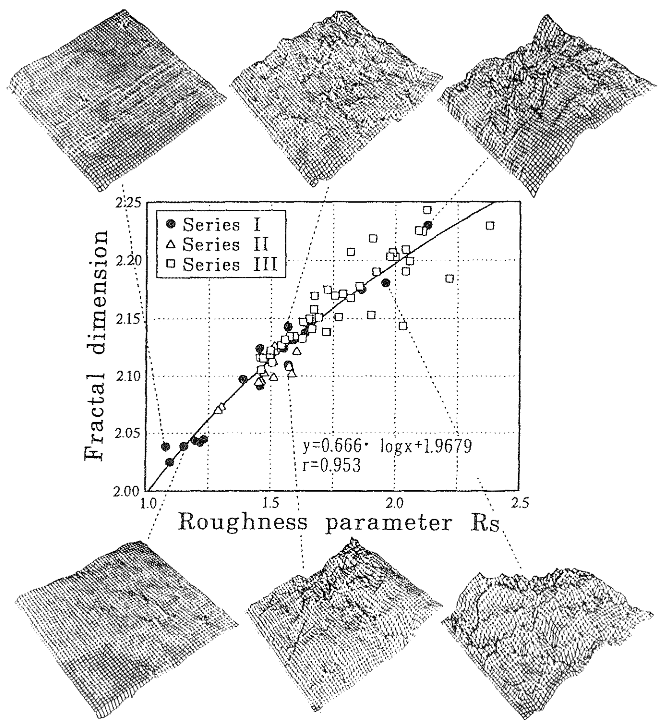

Fig.11 Relation between R_S and D_S

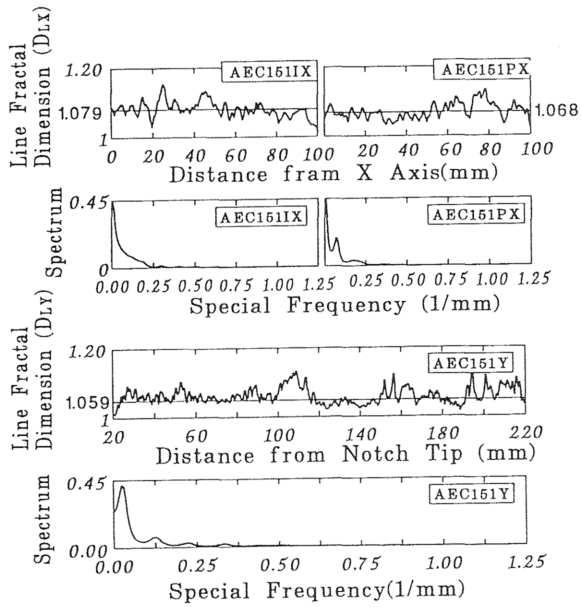

Fig.12 An example of line fractal dimension and spectrum

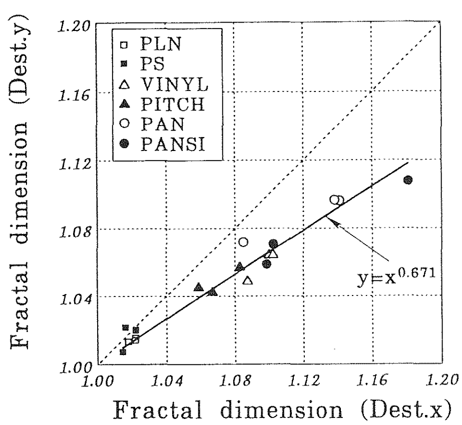

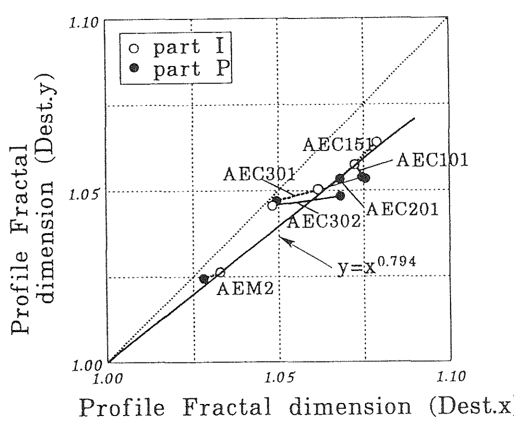

Fig.13 Relation between D_{LX} and D_{LY} in Series I

Fig.14 Relation between D_{LX} and D_{LY} in Series II

the most relevant parameter to describe the roughness of fracture surface, as shown in Fig. 11. While Rs is an average of the surface roughness and it is insensitive to the local rough surface, Ds is influenced even by such a local rough surface. On the other hand, D_L describe the surface roughness on the measured stripe. D_{Lx} is generally larger than D_{Ly} but both of them are almost the same in plain mortar and high

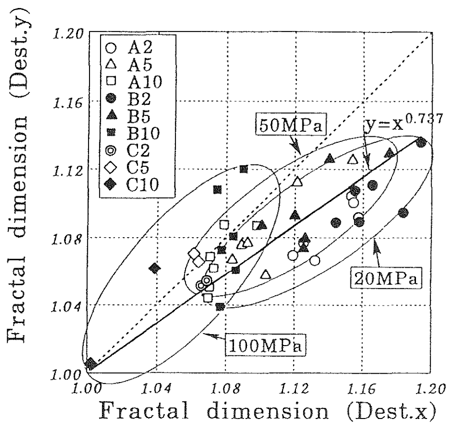

Fig.15 Relation between D_{Lx} and D_{Ly} in Series III

strength concrete. Fig. 12 shows an example of line fractal dimension and their spectrum properties. Fig. 13, 14 and 15 show relations between D_{Lx} and D_{Ly}. In all of these three series, each relation can be described as a power function whose exponent is rather closed each other.

Plots in Fig. 15 constitute three groups. Plots of high strength group (A10, B10 and C10) are diagonally distributed, though the scatter is rather large. On the other hand, plots of low strength group (A2, B2 and C2) are deviated from the diagonal. Plots of the third group of medium strength (A5, B5 and C5) are in the middle of these two groups. In other words, the ratio of D_{Lx} to D_{Ly} deviates further from the unity as the heterogeneity increases.

4.2 True surface area

It might be worthwhile to notice that two parameters in Fig. 11 are related very closely with a unique equation for totally different cementitious composite materials. Although the measured surface area depends on the adopted interval size, the analyzed fractal dimension is in principle independent of the size. Therefore the true surface area can be given as a function of Ds as follows:

$$S = A'\{\exp(Ds-1.97)\}^{1.50} \qquad (4)$$

4.3 Fractal dimension and toughness parameter

Ds is distributed within 2.038 and 2.229 in Series I, 2.069 and 2.125 in Series II, and 2.115 and 2.242 in Series III. While fracture surfaces of plain mortar are usually much flatter than those of other fiber reinforced mortar composites and concrete, it is reflected that the value of Ds for mortar is smaller than other composites and concrete. However, it has been failed so far in finding any quantitative relations between Ds and fracture mechanics parameters except one which is shown in Fig. 16. Fig. 16 shows a relation between (Ds-2) and an equivalent toughness $\sqrt{EG_F}$ in Series I. The reason why the toughness parameter of plain concrete is not related to Ds but fiber reinforced mortar does may be due to the degree of heterogeneity in the material structure.

G_F of plain concrete was strongly correlated with the total interface area but it was independent of roughness parameter of aggregates Ras as shown in Fig. 17. While a larger value of Ras means that aggregates are more deeply embedded into the matrix by which bridging mechanism works, no correlation between Ras and G_F may suggest that the energy absorption mechanism due to bridging of limited number of aggregates does not dominantly contribute to increase G_F of plain concrete but that

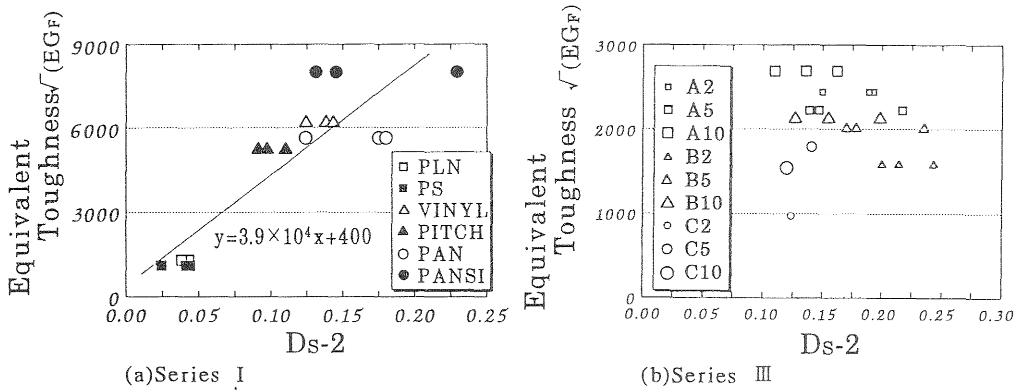

Fig.16 Relation between (Ds-2) and $\sqrt{EG_F}$

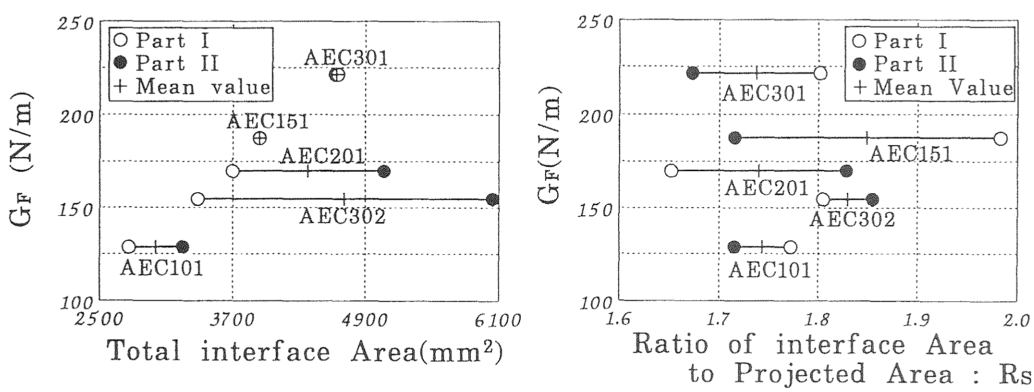

Fig.17 Relation between G_F and features of fracture surface

the deflection of cracks through interfaces is the main mechanism. Spectrum of D_{Ly} in Fig. 12 shows that more tortuous crack propagation absorbs larger amount of G_F.

On the basis of the fictitious crack model with a bilinear tension softening diagram, the inverse analysis of load-displacement curves was performed to determine essential four parameters: Ft, S_1, W_1 and Wc (Wittmann et al., 1987). As shown in Fig. 18, there seems to be a certain relation between Wc and D_{Lx} but no relations are recognized between Ds and Wc.

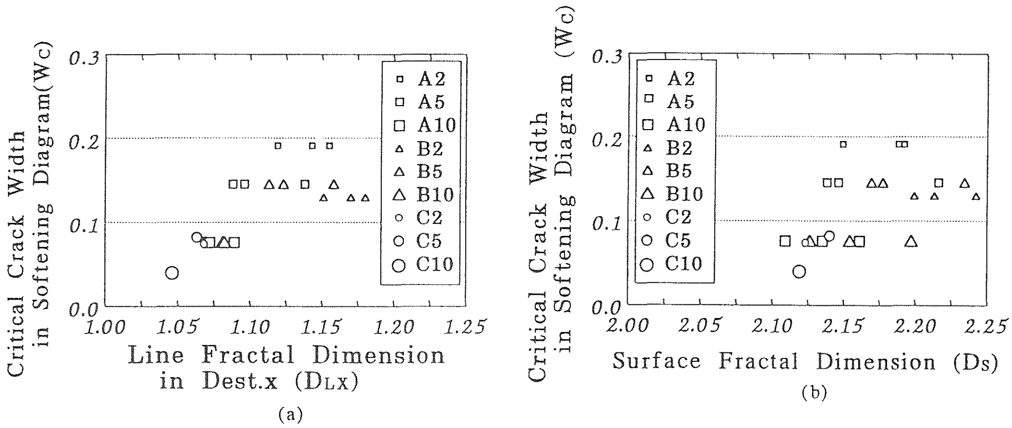

Fig.18 Relation between fractal dimension and W_C

4.4 Orientation of facets

As shown in Fig. 19 which is the frequency of θ in Series I, the peak

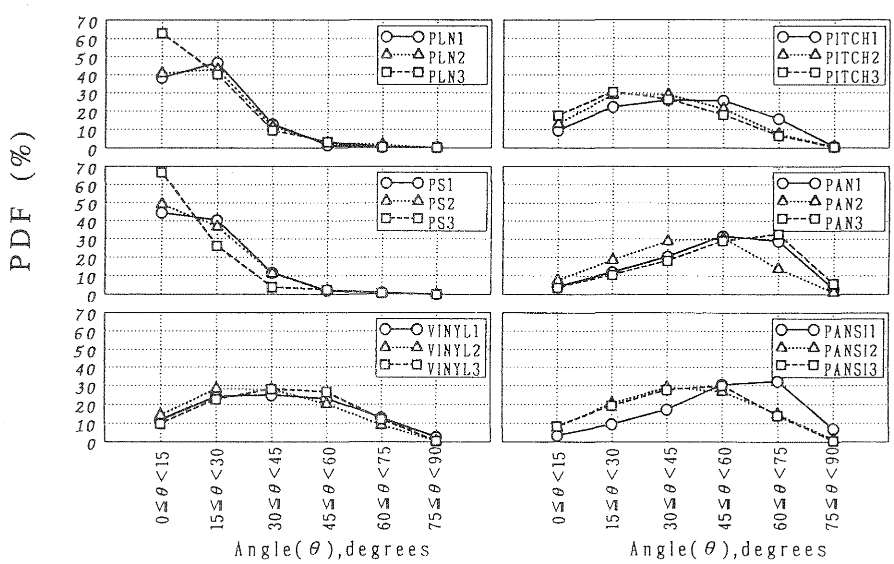

Fig.19 Frequency of facet orientation in Series I

value of θ shifts from 0° towards 90° as G_F increases. While the variation of θ was rather small in Series II, similar shifting tendencies of θ was recognized in Series III as the strength decreases.

ϕ distribution for plain mortar in Series I is classified into the group I but that for other fiber reinforced mortar in Series I and low strength concrete in Series III is done into group II defined in Fig. 6. Moreover ϕ distribution for high strength concrete in Series III is classified into group III.

5 Conclusions

Several parameters to analyze quantitatively features of fracture surfaces in various types of cementitious composite materials were presented. They are useful to study micromechanisms of the fracture especially for developing new cementitious materials. Further studies need to be done to relate these quantitative features to fracture mechanics parameters.

References

Mecholsky, J.J., Passoja, D.E. and Feinberg-Ringel, K.S. (1989) Quantitative analysis of brittle fracture surfaces using fractal geometry. **J. Am. Ceram. Soc.**, 71 [1], 60-65.

Mihashi, H. and Umeoka, T. (1993) Fracture properties of fiber reinforced cementitious composite materials, in **Proc. 3rd Japan Int. SAMPE Symposium** (ed. T. Kishi), 224-229.

Mihashi, H., Nomura, N. and Umeoka, T. (1994) Fracture mechanics parameters of cementitious composite materials and fractured surface properties, in **Fracture and Damage in Quasibrittle Structures** (eds Z.P. Bazant, Z. Bittnar, M. Jirasek and J. Mazars), E & FN Spon, London, 191-198.

Mihashi, H. and Nomura, N. (1992a) Microcracking and tension softening properties of Concrete, **Cem. Conc. Comp.**, 14, 91-103.

Mihashi, H., Kirikoshi, K. and Nomura, N. (1992b) Strength properties of FRC on the basis of fracture mechanics, in **High Performance Fiber Reinforced Cement Composites** (eds H.W. Reinhardt and A.E. Naaman), E & FN Spon, 313-324.

Otsuka, K. (1994) Size effect in fracture process zone of concrete, in **Size Effect in Concrete Structures** (eds. H. Mihashi,H.Okamura and Z.P.Bazant), E & FN Spon, 47-56.

RILEM 50-FMC (1985) Determination of the fracture energy of mortar and concrete by means of three-point bend test on notched beams, **Mater. Struct.**, 18, 285-290.

Underwood, E.E. and Banerji, K. (1986) Fractals in fractography, **Mater. Sci. Eng.**, 80, 1-14.

Van Mier, J.G.M. (1991) Crack face bridging in normal, high strength and lytag concrete, in **Fracture Processes in Concrete, Rock and Ceramics** (eds. J.G.M. van Mier, J.G. Rots and A. Bakker), E & FN Spon, London, 27-40.

Wittmann, F.H., Roelfstra,P.E., Mihashi,H.,Huang,Y.-Y.,Zhang,X.-H. and Nomura,N.(1987)Influence of age of loading, water-cement ratio and rate loading on fracture energy of concrete, **Mater. Struct.**, 20, 103-110.

Appendix Table A-1 Fractal dimension and roughness parameter of fracture surfaces

(1)Series I

specimen	Surface Fractal D.	Line fractal D. Dest.x	Dest.y	R_S	GF (N/m)
PLN1	2.038	1.018	1.013	1.079	60
PLN2	2.048	1.022	1.015	1.198	
PLN3	2.038	1.022	1.014	1.151	
PS1	2.044	1.022	1.020	1.230	41
PS2	2.041	1.016	1.021	1.216	
PS3	2.024	1.014	1.007	1.098	
VINYL1	2.138	1.100	1.064	1.637	1443
VINYL2	2.124	1.087	1.049	1.455	
VINYL3	2.143	1.102	1.064	1.567	
PITCH1	2.110	1.141	1.096	1.568	1110
PITCH2	2.091	1.059	1.045	1.457	
PITCH3	2.097	1.067	1.042	1.388	
PAN1	2.175	1.141	1.096	1.863	2411
PAN2	2.124	1.085	1.072	1.552	
PAN3	2.180	1.138	1.097	1.961	
PANSI1	2.229	1.181	1.108	2.129	2080
PANSI2	2.131	1.099	1.059	1.590	
PANSI3	2.145	1.102	1.071	1.653	

(2)Series II

Specimen	Surface Fractal D.	Line fractal D. Dest.x	Dest.y	R_S	G_F (N/m)
AEM2I	2.072	1.033	1.027	1.301	103
AEM2P	2.069	1.028		1.288	
AEC101I	2.121	1.072	1.056	1.516	129
AEC101P	2.125	1.074		1.515	
AEC151I	2.120	1.079	1.059	1.605	187
AEC151P	2.112	1.068		1.509	
AEC201I	2.102	1.062	1.052	1.473	170
AEC201P	2.107	1.076		1.573	
AEC301I	2.098	1.062	1.049	1.510	221
AEC301P	2.095	1.049		1.461	
AEC302I	2.094	1.048	1.047	1.451	155
AEC302P	2.102	1.068		1.584	

(3)Series III

Specimen	Surface Fractal D.	Line fractal D. Dest.x	Dest.y	R_S	G_F (N/m)
A2-1	2.149	1.119	1.074	1.966	265
A2-2	2.192	1.155	1.099	2.137	176
A2-3	2.188	1.143	1.084	1.930	121
A5-1	2.138	1.096	1.067	1.722	124
A5-2	2.216	1.138	1.119	2.188	125
A5-3	2.146	1.088	1.072	1.678	118
A10-1	2.109	1.071	1.048	1.482	131
A10-2	2.161	1.089	1.088	1.780	129
A10-3	2.135	1.072	1.066	1.610	139
B2-1	2.213	1.170	1.102	1.948	93
B2-2	2.242	1.180	1.124	2.200	78
B2-3	2.199	1.151	1.089	1.894	89
B5-1	2.169	1.113	1.081	1.715	-
B5-2	2.234	1.158	1.128	2.110	106
B5-3	2.177	1.123	1.086	1.791	115
B10-1	2.154	1.081	1.077	1.664	88
B10-2	2.197	1.082	1.114	1.950	95
B10-3	2.126	1.082	1.050	1.515	107
C2-1	2.123	1.068	1.053	1.518	46
C5-2	2.140	1.063	1.053	1.592	95
C10-2	2.119	1.046	1.062	1.484	59